Progress In Electromagnetics Research, Vol. 116, 137–157, 2011

USE OF HIGH-IMPEDANCE SCREENS FOR ENHANCING ANTENNA PERFORMANCE WITH ELECTROMAGNETIC COMPATIBILITY

M.-S. Lin

Department of Electrical Engineering
National Yunlin University of Science and Technology
No. 123, Section 3, University Road, Douliou, Yunlin 64002
Taiwan, R.O.C.

C.-H. Huang

Graduate School of Engineering Science and Technology
National Yunlin University of Science and Technology
No. 123, Section 3, University Road, Douliou, Yunlin 64002
Taiwan, R.O.C.

C.-N. Chiu

Department of Electrical Engineering
Da-Yeh University
No. 168, University Road, Dacun, Changhua 51591, Taiwan, R.O.C.

Abstract—When developing a wireless communication system, a designer should consider the associated radiated power density, electromagnetic compatibility (EMC), and specific absorption rate (SAR). In this paper, high-impedance surfaces (HISs) are designed as an EM protection screen to reduce the interaction between an antenna and the user behind the screen. The effects of an HIS screen with a finite number of cells placed near a monopole antenna for the application of the 2.4 GHz WLAN band were thoroughly investigated. The screen is first-ever proposed not only to reduce the backward radiation from the antenna, but also to shift the impedance-matching band of the antenna and to adjust the corresponding bandwidth. As a result, the SAR behind the screen is noticeably lowered, and the out-of-band spurious emission from the antenna can be reduced. Two typical kinds of HIS structures, mushroom-shaped and Jerusalem

Received 4 March 2011, Accepted 26 April 2011, Scheduled 2 May 2011
Corresponding author: Ming-Shing Lin (starlin@yuntech.edu.tw).

Cross HISs (abbreviated as MSHIS and JCHIS, respectively), were investigated by numerical simulations and measurements. Three different measurement techniques were proposed for predicting the operating frequency band of an HIS. Some HIS-added antenna prototypes were constructed and studied. It was found that the MSHIS and JCHIS can adjust the impedance-matching band of the antenna, do not affect the radiation performance in the forward direction, and can significantly reduce the backward radiated power. In addition, the measured maximum SAR has been significantly reduced from 0.976 W/kg for the monopole antenna without an HIS to 0.037 and 0.038 W/kg, respectively, for the antenna with an MSHIS and a JCHIS.

1. INTRODUCTION

In recent years, many wireless communication systems have been rapidly developed. They include universal mobile telecommunications system (UMTS), wireless local area network (WLAN), Bluetooth, and long-term evolution (LTE) of Third Generation Partnership Project (3GPP), to name only a few. In all these systems, the effects of electromagnetic (EM) radiation on human bodies have become an important research topic in the area of electromagnetic compatibility (EMC). In IEEE Std C95.1 [1], ICNIRP Guidelines [2], FCC OET Bulletin 65C [3], IEC62209-1 [4], and IEEE Std 1528 [5], recommendations (or restrictions) and measurement procedures have been made available to ensure the EM radiation safety of wireless communication devices and to protect human bodies against adverse health effects resulting from EM exposure. In order to pass the requirements of existing standards or regulations for the wireless devices, a designer should consider the radiated power density, electromagnetic compatibility (EMC), and specific absorption rate (SAR) of these devices [6, 7]. In addition to EMC and radiation hazard issues, the designer should also minimize the influence of any nearby user's body on the performance of the antennas mounted on theses devices and promote the quality of communications [8–12].

The performance of wireless antennas is usually affected significantly by the presence of nearby conductors or human bodies because conductive surfaces will reverse the phase of the reflected wave and support the propagation of surface waves. In contrast, an HIS structure does not reverse the phase of a reflected wave and can prohibit the propagation of surface waves in a forbidden frequency band [13]. Therefore, if the operating frequency is within the resonant band of the HIS structure, one can use the HIS structure to reduce the interaction between the antenna of a wireless communication device

and its user. In recent years, high-impedance surfaces (HISs) [13–15] and frequency selective surfaces (FSSs) [16–18] have been introduced in the design of antennas [19–25], EMC [10, 26–28], and microwave circuits.

In this study, HISs were employed as an electromagnetic protection screen. The screen is newly proposed not only to reduce the interaction between the antenna of a communication device and its user, and to reduce the SAR, but also to adjust the impedance-matching band of the antenna and to lower the out-of-band spurious emission from the device. For illustration, the mushroom-shaped HIS (MSHIS) and the Jerusalem Cross HIS (JCHIS) structures were designed in the 2.4 GHz WLAN band. In addition, monopole antennas are employed in this study, for they are easy to fabricate and widely used.

First, the resonant band of each HIS for the TE and TM incidences was investigated by numerical analysis. It was found that the resonant frequency of the MSHIS (JCHIS) will increase (decrease) as the incident angle increases. Three measurement methods, the electric field probe method [14], microstrip line method [19], and GTEM method [28], were proposed and compared to verify the performance of each HIS having a finite number of cells (abbreviated as finite HIS). Next, the effects of the cell number of each HIS on the performance of the HIS-added monopole antenna were studied, and the scaling factors of the MSHIS and JCHIS were obtained for rapidly fine tuning the HISs as they are added to the antenna. Finally, the return loss and radiation pattern of the HIS-added monopole antenna were investigated. The effects of the HIS screens on the antenna were also illustrated by radiation power and SAR values. Measured results indicate that these two HIS structures can be used as an electromagnetic protection screen to reduce the SAR without affecting the forward radiating power of the antenna.

2. CONFIGURATION OF HIS-ADDED MONOPOLE ANTENNA

Figure 1 shows the configuration of a cylindrical monopole antenna with a high-impedance screen below. The monopole antenna designed for the 2.4 GHz WLAN band consists of a cylindrical wire and a 50-Ω microstrip feed line. The former has a length (L_A) of 28 mm and a diameter (W_A) of 3.06 mm; the latter is printed on a grounded FR4 substrate with a dielectric constant of 4.4, a loss tangent of 0.02, a thickness (t_1) of 1.6 mm, a width (W_B) of 60 mm, and a length (L_B) of 100 mm. For convenience, refer to this grounded substrate as a PCB.

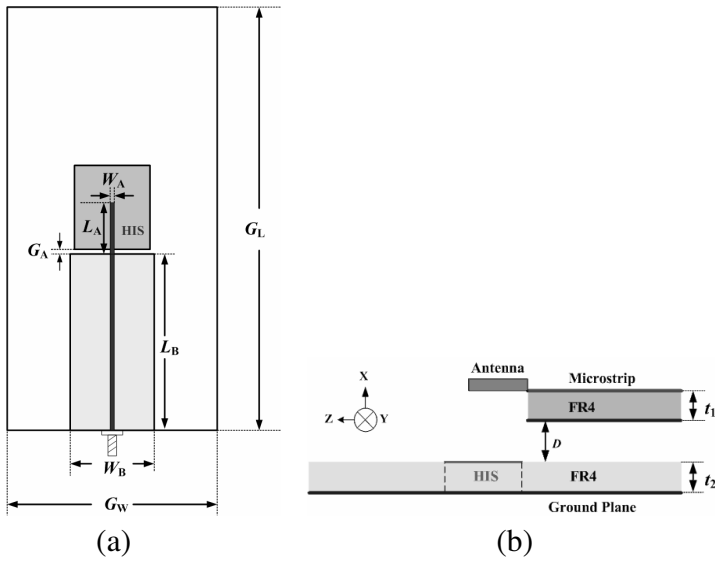

Figure 1. Configuration of a monopole antenna with a high-impedance screen: (a) top view, (b) side view.

Below the PCB is another grounded FR4 substrate on which the HIS structure resides and for which the thickness (t_2), width (G_W), and length (G_L) are 0.8, 150, and 300 mm, respectively. In this study, the PCB is stacked right on the top of the lower grounded substrate; in other words, $D = 0$ mm in Fig. 1. When projected onto the same plane, the PCB and the HIS have a gap (G_A) of 0.2 mm in between. Details of the MSHIS and JCHIS will be presented in the next section.

3. INVESTIGATION ON THE PERFORMANCE OF HIS

Figures 2(a) and 2(b) show the geometries of the 2×2 cells of the MSHIS and JCHIS, respectively, designed for the 2.4 GHz band. In each cell of the MSHIS, the rectangular patch with a side length (w) of 27.7 mm is loaded at the center by a conducting via of diameter $d = 1$ mm and is separated from the patch in the adjacent cell by a gap (g) of 0.8 mm, leading the period (a) of the MSHIS to 28.5 mm. The JCHIS, having the same period as that of the MSHIS, can be regarded as a frequency-selective-surface-based structure. Other structural dimensions of the JCHIS are $I = 4.6$, $W_s = 2$, $L_S = 10.85$, and $g = 0.8$, all in millimeter.

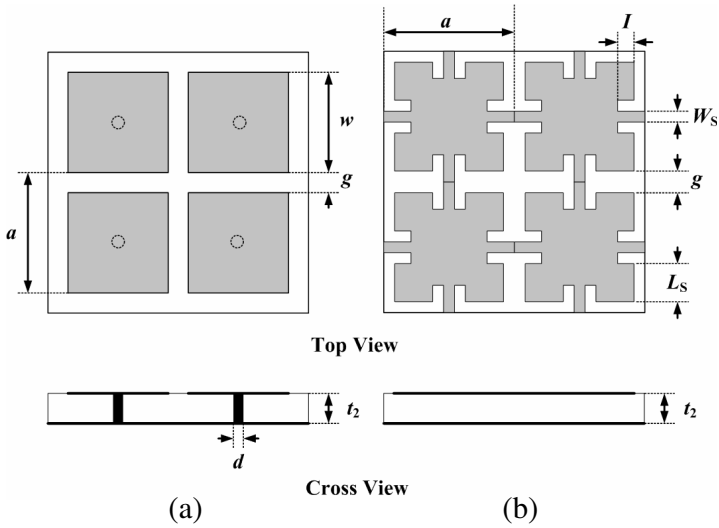

Figure 2. Geometry of high impedance surfaces designed for 2.4-GHz band: (a) MSHIS, (b) JCHIS.

3.1. Numerical Study of HIS Performance

In order to approximately and efficiently predict the complex performance of the finite MSHIS and JCHIS placed very near an antenna, the plane-wave reflections from the MSHIS and JCHIS with infinitely many cells (called infinite MSHIS and JCHIS, respectively, for short) were simulated and studied at first. These simulations were conducted by using the software Ansoft HFSS incorporating with a periodic boundary condition [29]. The simulation configuration of either infinite HIS obliquely illuminated by a plane wave is shown in Fig. 3. Both the TE and TM incidence are considered and the incident angle (θ) was widely varied for clearly illustrating the HIS performance as follows.

Figures 4(a) and 4(b) show the simulated phase of the reflection coefficient ($\angle S_{11}$, called the reflection phase for short) of the MSHIS and JCHIS for the TE polarizations, respectively. The structural dimensions of these infinite HISs are the same as those of the finite HISs in Fig. 2. Results simulated for the TM polarizations are similar and hence will not be presented here for conciseness. In the results of the normal incidence ($\theta = 0°$), it is found that the MSHIS has a resonant frequency (defined as the frequency at which $\angle S_{11} = 0°$) at 2.44 GHz and resonant band (defined as the frequency range in which $-90° \leq \angle S_{11} \leq 90°$) from 2.40 to 2.48 GHz. However, JCHIS

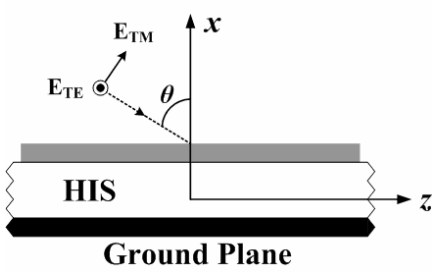

Figure 3. Configuration of the infinite HIS obliquely illuminated by a plane wave.

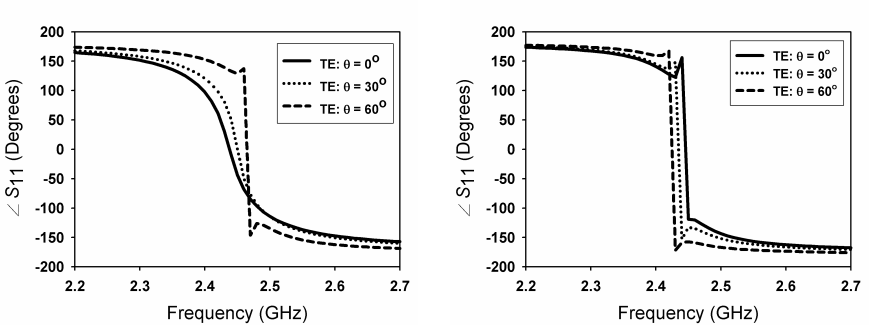

Figure 4. Simulated reflection phase of the HIS for the TE incidences at different incident angles: (a) MSHIS, (b) JCHIS.

has a resonant frequency at 2.44 GHz and resonant band from 2.43 to 2.45 GHz. The simulated results show that the resonant band of the MSHIS is wider than that of the JCHIS. In the results of oblique incidences, one can also find that the resonant frequency of the MSHIS (JCHIS) will increase (decrease) as the incident angle increases. The slopes of the reflection phase of the MSHIS and JCHIS near the resonance become steeper as the incident angle increases.

3.2. Test Methods for Verifying the Performance of HISs

The insertion loss ($-20\log_{10}|S_{21}|$) of the wave transmission and the reflection phase ($\angle S_{11}$) can be used to characterize the performance of HIS structures. In this study, the electric field probe method [14], microstrip line method [19] and GTEM method [28], are proposed to determine the performance of finite HISs. Fig. 5 shows the test configurations of three methods.

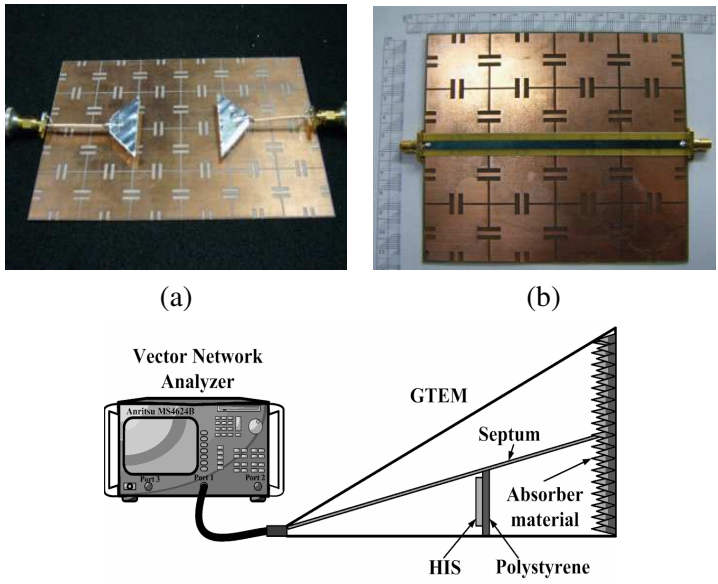

Figure 5. Test configuration of performance measurement for HISs: (a) electric field probe method, (b) microstrip line method, (c) GTEM method.

A photograph of the electric field probe method is shown in Fig. 5(a). Two triangular parallel plate antennas that excite vertical electric field are connected to a network analyzer, and the insertion loss of the TM surface-wave transmission [14] across the HIS structure is measured. The insertion loss of the wave transmission can be used to determine the band gap of the HIS. Fig. 5(b) shows the photograph of the microstrip line method. A 50-Ω microstrip transmission line is printed on the top of the ungrounded FR4 substrate. The substrate is placed on an HIS structure; the two ports of the transmission line are connected to the network analyzer. The insertion loss of the microstrip line can be used to determine the band gap of HIS [19]. Shown in Fig. 5(c) is the test configuration of the reflection phase method. This method uses a GTEM cell to measure reflection phase of the HIS plate. First, the reflection phase of a finite-thickness metal sheet with the same dimension as the HIS plate is measured as the reference. Second, the HIS plate is located such that the position of its front surface is the same as that of the metal sheet's surface facing the incident wave. Next, the reflection phase so measured is normalized by the

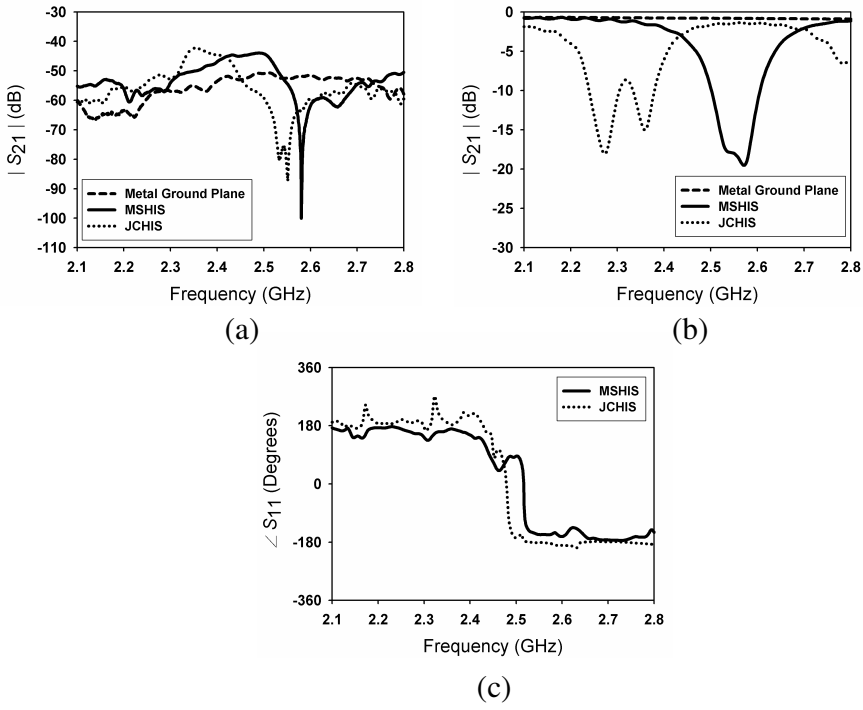

Figure 6. Measured results of the metal ground plane, MSHIS and JCHIS by the method of (a) electric field probe, (b) microstrip line, (c) GTEM.

one obtained in the first step. This leads to $\angle S_{11} - 180^\circ$ of the HIS plate with the plate's front surface as the reference plane (i.e., the propagation phase factor of the signal path between the vector network analyzer and the HIS plate under investigation is cancelled). Last, the reflection phase ($\angle S_{11}$) of the HIS plate can be obtained by adding back 180°.

Measured results of the metal ground plane, MSHIS and JCHIS by three methods are shown in Fig. 6. From the results, the resonant frequency of the MSHIS (or JCHIS) is estimated to be 2.58 GHz (or 2.55 GHz) from the electric probe method, 2.57 GHz (or 2.27 GHz) from the microstrip line method, and 2.52 GHz (or 2.48 GHz) for GTEM method. Because GTEM can generate local plane wave for the measurement, the results of GTEM measurement are close to the simulation results (2.44 GHz for both HISs) in the case of normal plane-wave incidence. It was found that GTEM method has the best

prediction for the resonant frequencies of HISs. However, microstrip line method can provide better information for frequency bandwidth of HISs. In addition, the later results will show that the microstrip line method can especially predict the band shifting effect of an antenna while these HISs are closely placed.

4. APPROACH TO DESIGNING HIS-ADDED ANTENNAS

In reality, the number of cells in an HIS on the back of the monopole antenna should be as small as possible for the HIS-added antenna to be of practical value. However, the number of cells may affect the performance of the HIS-added antenna [24]. We then have to determine the number of cells needed first. On the other hand, the operating band of the HIS-added antenna with a given number of cells may occur at a band different from the resonant band of the infinite HIS. Since the dimensions of the HIS are initially determined from the simulated results for the infinite HIS, it is thus necessary that a scaling factor be obtained after comparing the operating band of the HIS-added antenna and the resonant band of the infinite HIS. With the scaling factor available, the dimensions of the finite HIS are scaled accordingly so that the operating band of the HIS-added antenna can be shifted to the desired frequency location. Finally, the HIS-added antenna so designed is evaluated in terms of return loss, radiation pattern, forward radiated power (FRP), backward radiated power (BRP), and SAR.

4.1. Effect of Cell Numbers

Figure 7 shows the $|S_{11}|$ of the monopole antenna itself and the HIS-added monopole antenna with several different numbers of cells. As far as the operating band for the 2.4 GHz WLAN (determined by $|S_{11}| \leq -10$ dB) is concerned, the optimal number of cells for both the MSHIS-added antenna and the JCHIS-added one is 2×2. Hence, in what follows the MSHIS- and JCHIS-added monopole antennas are meant to have 2×2 cells, unless otherwise specified. Before the HIS is added, the designed monopole antenna itself is a wideband antenna having a simulated $|S_{11}| \leq -10$ dB impedance band of 2.04–2.77 GHz that corresponds to a fractional bandwidth of 30.4% with respect to the center frequency 2.405 GHz. Such a large bandwidth is improper and may cause out-of-band spurious emissions. With the MSHIS (JCHIS) of 2×2 cells added, the impedance band narrows to 2.46–2.61 GHz (2.28–2.36 GHz) with a center frequency of higher (lower) than 2.405 GHz. Clearly, the impedance bandwidths of both

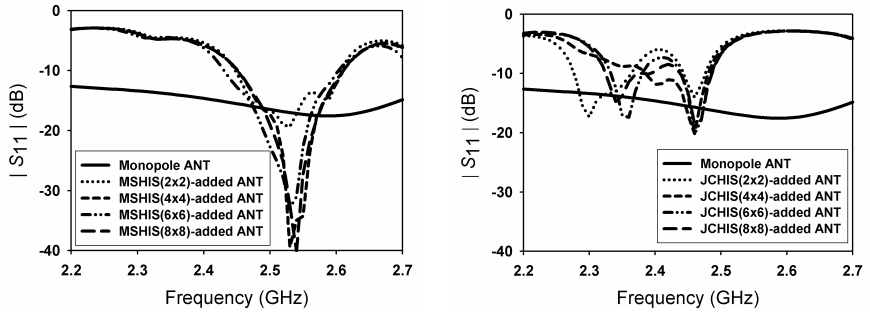

Figure 7. Simulated $|S_{11}|$ of the HIS-added antenna with the number of cells as a parameter: (a) MSHIS, (b) JCHIS.

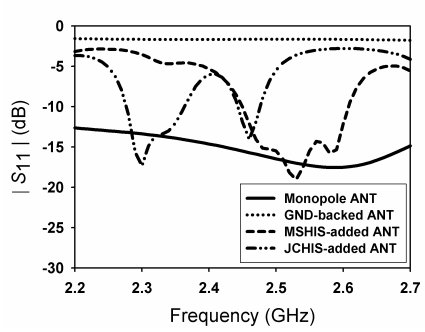

Figure 8. Simulated $|S_{11}|$ of the HIS-less monopole antenna, the ground-plane-backed antenna, the MSHIS-added antenna, and the JCHIS-added antenna.

the MSHIS- and JCHIS-added antennas are significantly reduced and more optimal as compared with that of the HIS-less monopole antenna. Nevertheless, the MSHIS seems to have more stable influence on the monopole antenna than the JCHIS as the number of cells is varied.

4.2. Scaling Factor of MSHIS and JCHIS Used for Monopole Antenna

Figure 8 shows the simulated $|S_{11}|$ of the HIS-less monopole antenna, the MSHIS-added antenna, the JCHIS-added antenna, and the antenna with the top surface of the supporting substrate ($G_W \times G_L$ in Fig. 1) completely printed with a grounded metal plane (called ground-plane-

backed antenna for short). For the case of the ground-plane-backed antenna, since the monopole radiator is parallel to and very close to the ground plane, the wave radiated into the upper half space by the monopole radiator is almost cancelled by the wave radiated onto and then reflected from the grounded plane. This in effect results in little real power radiated by the monopole radiator, thus leading to a small return loss in the displayed frequency range of 2.2–2.7 GHz. On the other hand, it is expected that if with infinitely many cells, the HIS-added antenna should have the operating band near the resonant band of the HIS since inside that resonant band the reflected from the HIS will not cancel the wave directed into the half space. However, for our MSHIS-added (JCHIS-added) antenna with a finite number of cells, the operating band of 2.45–2.60 (2.28–2.36) GHz has a fractional bandwidth of 5.9% (3.4%) with respect to the center frequency 2.525 (2.32) GHz. The center frequencies of the operating bands slightly deviate from the resonant-band center frequencies of the infinite HISs. For practical purpose and from the design point of view, the deviations can be offset easily by scaling the structural dimensions of the finite HISs. For that purpose, we can define a scaling factor as $\alpha = f_a/f_d$, where f_a is simulated frequency at which the HIS-added monopole antenna has a minimum $|S_{11}|$ (or a maximum return loss), and f_d is desired resonant-band center frequency of the infinite HIS under normal plane-wave incidence. In this study, the $f_d = 2.45$ GHz for WLAN band.

In the structural scaling process for the finite HIS, the structural parameters obtained for the infinite HIS should be multiplied by the scaling factor just computed. Because commercial microwave

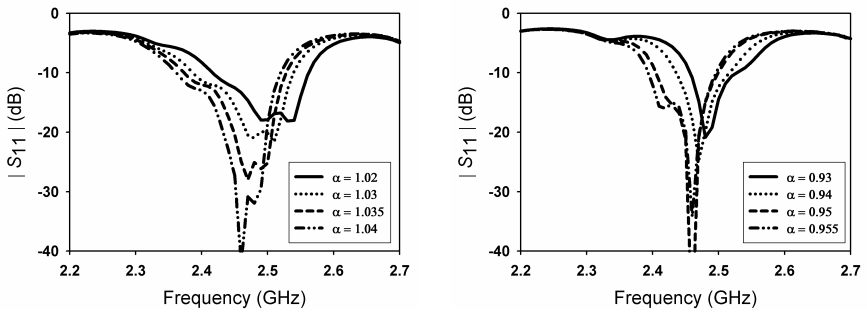

Figure 9. Simulated $|S_{11}|$ of the scaled. (a) MSHIS- and (b) JCHIS-added antennas for several different scaling factors.

substrates of the same substance that can be acquired have only a few different thicknesses and available commercial cylindrical conductors used as the vias in the MSHIS have only some discrete radii, the parameters t_2 and d (see Fig. 2) will be set unchanged in the scaling process. For simplicity, $G_W \times G_L$ will neither be scaled. Hence, such a scaling process using the scaling factor just computed may not lead the HIS-added monopole antenna to having a satisfactory new operating band. In that case, we should further fine tune the structural dimensions of the finite HIS until a satisfactory operating band is obtained. Alternatively, we can perform the simulations for a set of scaling factors around the one computed above and then choose the one that leads to a satisfactory new operating band for fabrication.

From Fig. 8, the smallest $|S_{11}|$ of -19.06 (-17.33) dB occurs at 2.53 (2.3) GHz for the MSHIS-added (JCHIS-added) antenna, leading to a scaling factor (α) of 1.03 (0.94). Figs. 9(a) and 9(b) show the simulated $|S_{11}|$ of the scaled MSHIS- and JCHIS-added antennas, respectively, for several different scaling factors. For the MSHIS-added antenna, the initially computed $\alpha = 1.03$ has already provided satisfactory results, with the new structural parameters and the resulting operating band summarized in Table 1. In contrast, for the JCHIS-added antenna, the initially computed $\alpha = 0.94$ does not result in desired operating band. Close scrutiny of Fig. 9(b) reveals that with α changed to 0.955 satisfactory performance of the JCHIS-added antenna can be obtained, with the new structural parameters and the resulting operating band summarized in Table 2.

Table 1. New structural parameters and simulated operating band of the scaled MSHIS-added monopole antenna.

α	w (mm)	g (mm)	a (mm)	Operating band
1.03	28.53	0.82	29.35	2.39–2.54 GHz

Table 2. New structural parameters and simulated operating band of the scaled JCHIS-added monopole antenna.

α	W_s (mm)	g (mm)	L_s (mm)	a (mm)	Operating band
0.955	1.91	0.76	10.36	27.22	2.40–2.49 GHz

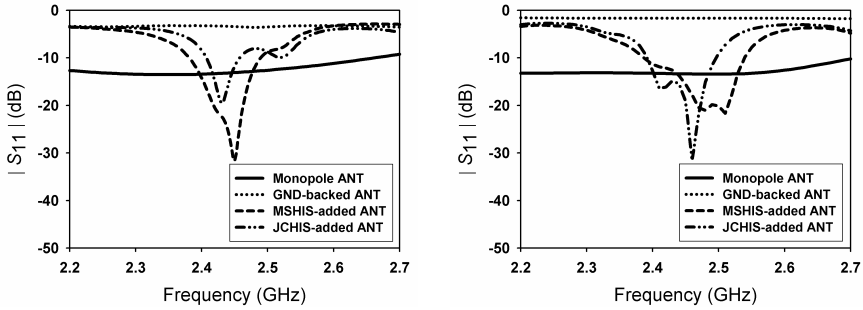

Figure 10. (a) Measured and (b) simulated $|S_{11}|$ of the HIS-less monopole antenna, the ground-plane-backed antenna, the MSHIS-added antenna, and the JCHIS-added antenna.

4.3. Simulated and Measured Results of HIS-added Monopole Antenna

Figure 10(a) shows the measured $|S_{11}|$ of the HIS-less monopole antenna, the ground-plane-backed antenna, the scaled MSHIS-added antenna, and the scaled JCHIS-added antenna. For comparison, the simulated results of the same antennas are also shown beside (Fig. 10(b)), and important parameters are also summarized in Table 1 and Table 2. The MSHIS-added antenna has the simulated return loss of -21.64 dB (at 2.51 GHz) with a fractional bandwidth of 6.1% from 2.39 to 2.54 GHz, and has the measured return loss of -31.64 dB (at 2.45 GHz), with a fractional of 4.5% from 2.38 to 2.49 GHz. The JCHIS-added antenna has the simulated return loss of -31.59 dB (at 2.46 GHz) with a fractional bandwidth of 3.7% from 2.4 to 2.49 GHz, and has the measured return loss of -19.50 dB (at 2.43 GHz) with a fractional bandwidth of 2.5% from 2.40 to 2.46 GHz. Because of the narrow resonant bands of the HISs, the operating bands of the HIS-added antennas have been narrowed from that of the HIS-less monopole antenna. Since the resonant band of the infinite MSHIS is wider than that of the infinite JCHIS (see Fig. 4), it is of no surprise that the operating band of the scaled MSHIS-added antenna is also wider than that of the scaled JCHIS-added antenna. Unfortunately, the measured operating band of 2.40–2.46 GHz for the latter is not wide enough to completely cover the desired WLAN band of 2.4–2.484 GHz [30].

The advantages of the embedded HIS in the HIS-added antenna are twofold. First, the out-of-band emissions from the monopole radiator can be reduced, thus lowering the annoyance pertaining to

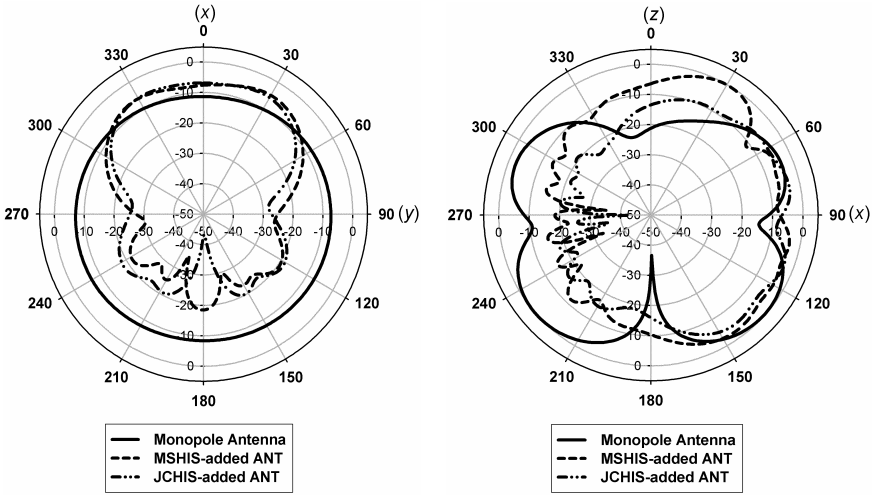

(a) (b)

Figure 11. Simulated normalized co-polarized radiation patterns of the monopole antenna and the scaled HIS-added antennas at 2.45 GHz: (a) xy-plane, (b) xz-plane.

EMC. Second, in the operating band, the presence of the HIS can reduce the backward radiation and thus the SAR, without sacrificing the forward radiation characteristics of the HIS-less monopole antenna, as will be clear from the radiation patterns and powers to be presented below.

Figure 11 plots the simulated normalized radiation patterns of the scaled HIS-added antennas at 2.45 GHz. Clearly, the forward radiations (i.e., the radiations paraxial to the $+x$ direction) of the scaled HIS-added remain similar to that of the HIS-less monopole antenna itself. In contrast, the backward radiations (i.e., the radiations paraxial to the $-x$ direction) of the scaled HIS-added are significantly reduced from that of the HIS-less monopole antenna alone, implying that the SARs of the former can be greatly reduced from that of the latter.

To further illustrate what is claimed above, the forward horizon radiated power (FHRP), backward horizon radiated power (BHRP), forward radiated power (FRP), and backward radiated power (BRP) for the antennas under investigations are defined in this study. These definitions follow the total radiated power (TRP) and near-horizon radiated power (NHRP) that, for the purpose of evaluating the radiation performance of a mobile wireless product, have been introduced in CTIA Test Plan [31]. Note that the NHRP is used

to determine the power radiated near the azimuth axis. In computing these powers to be defined shortly, the effective isotropic radiation power, $\mathrm{EiRP}(\theta, \phi)$, taken at discrete positions on a complete sphere is needed.

Assume that the data of $\mathrm{EiRP}(\theta, \phi)$ are simulated or measured with N angular intervals in theta (θ) from 0 to π and M angular intervals in phi (ϕ) from 0 to 2π. Thus, $\mathrm{EiRP}(\theta_i, \phi_j)$ is referred to as the sample evaluated at $\theta_i = (180^\circ/N) \times i$ and $\phi_j = (360^\circ/M) \times j$, where $i = 0, 1, \ldots, N-1$ and $j = 0, 1, \ldots, M-1$. In this study, the elevation angular interval is specified as 15° ($N = 12$), and the azimuth angular interval is specified as 1° ($M = 360$). Then, the $\mathrm{FHRP}_{\pm 30}$, $\mathrm{BHRP}_{\pm 30}$, FRP, and BRP can be defined as follows:

$$\mathrm{FHRP}_{\pm 30} \cong \frac{\pi}{2NM}\left(\frac{\mathrm{FCut}_4 + \mathrm{FCut}_8}{2} + \sum_{i=5}^{7} \mathrm{FCut}_i\right) \tag{1}$$

$$\mathrm{BHRP}_{\pm 30} \cong \frac{\pi}{2NM}\left(\frac{\mathrm{BCut}_4 + \mathrm{BCut}_8}{2} + \sum_{i=5}^{7} \mathrm{BCut}_i\right) \tag{2}$$

$$\mathrm{FRP} \cong \frac{\pi}{2NM} \sum_{i=1}^{11} \mathrm{FCut}_i \tag{3}$$

$$\mathrm{BRP} \cong \frac{\pi}{2NM} \sum_{i=1}^{11} \mathrm{BCut}_i \tag{4}$$

where

$$\mathrm{FCut}_i = \left\{\sum_{j=0}^{89} + \sum_{j=270}^{359}\right\} [\mathrm{EiRP}_\theta(\theta_i, \phi_j) + \mathrm{EiRP}_\phi(\theta_i, \phi_j)] \sin\theta_i$$

and

$$\mathrm{BCut}_i = \sum_{j=90}^{269} [\mathrm{EiRP}_\theta(\theta_i, \phi_j) + \mathrm{EiRP}_\phi(\theta_i, \phi_j)] \sin\theta_i$$

represent the weighted sum of each conical cut.

Among these four terms, $\mathrm{FHRP}_{\pm 30}$ and FRP are related to the maximum communication distance between the wireless device and the base station, and $\mathrm{BHRP}_{\pm 30}$ and BRP pertain to the SAR of the wireless device. Ideally, the antenna should be designed to provide enough forward radiated power with lower backward radiated power. In these expressions, the effective isotropic radiation power is defined by $\mathrm{EiRP}(\theta, \phi) = P_T G_T(\theta, \phi)$, where $P_T G_T$ is the product of the transmitting power and the antenna's power gain. According to FCC

Table 3. FRP, BRP, $FHRP_{\pm 30}$, and $BHRP_{\pm 30}$ of monopole antenna and HIS-added antennas at 2.45 GHz.

	Monopole ANT (dBm)	MSHIS-added ANT (dBm)	JCHIS-added ANT (dBm)
FRP	26.11	25.67	25.00
BRP	26.55	16.11	15.28
$FHRP_{\pm 30}$	22.28	22.32	22.69
$BHRP_{\pm 30}$	22.99	11.27	12.19

Part 15 regulations [32], the maximum allowed P_T is 1 W for the 2.4 GHz WLAN band. With this P_T and the simulated antenna power gains (G_T), the $FHRP_{\pm 30}$, $BHRP_{\pm 30}$, FRP, and BRP of the monopole antenna and HIS-added antennas can be readily computed using Eqs. (1)–(4). The FRP, BRP, $FHRP_{\pm 30}$, and $BHRP_{\pm 30}$ at 2.45 GHz are summarized in Table 3. Clearly, the FRP and $FHRP_{\pm 30}$ of the MSHIS- and JCHIS-added antennas are close to those of the monopole antenna. On the other hand, the BRP and $BHRP_{\pm 30}$ of the MSHIS- and JCHIS-added antennas are approximately 10 dB smaller than those of the monopole antenna. This indicates that the HIS can serve as an electromagnetic protection screen without affecting the forward radiation power of the antenna.

The SAR is defined as the rate at which energy is absorbed per unit mass in a biological body exposed to an RF field [5]. The basic restrictions for whole body average SAR and localized SAR are given in ICNIRP Guideline [2] and FCC OET Bulletin 65, Supplement C [3]. The SAR in a biological body exposed to an RF field depends on the tissue geometry, dielectric properties, and the orientation of the body relative to the wireless device. Under normal gesture that a human body holding a wireless device, the BRP and $BHRP_{\pm 30}$ are the key factors affect the SAR. Because the BRP and $BHRP_{\pm 30}$ of the HIS-added antennas are reduced by approximately 10 dB as compared than those of the monopole antenna, we expect that the HIS should also effectively reduce the SAR of the monopole antenna without an HIS.

To verify that the HIS structure can be used as an electromagnetic protection screen, the SARs of the HIS-added monopole antenna are measured and compared with those of the HIS-less monopole antenna. The SAR measurements were carried out using an Aprel ALSAS 10 SAR testing system [33] with the orientations of the antenna under test and the phantom model shown in Fig. 12. With the input power set at 20 mW at 2.45 GHz, the measured results are summarized in Table 4. The SARs of the monopole antenna are 0.976 W/kg in a 1-g

(a) (b)

Figure 12. SAR test configuration: (a) Aprel ALSAS 10 SAR testing system, (b) the orientation of antenna and phantom model.

Table 4. SAR values of monopole antenna and HIS-added monopole antennas.

Product	Input power (mW)	Max. SAR 1-g Tissue (W/kg)	Max. SAR 10-g Tissue (W/kg)
Monopole ANT	20	0.976	0.578
Patch ANT	20	0.036	0.030
MSHIS-added ANT	20	0.037	0.031
JCHIS-added ANT	20	0.038	0.036

tissue and 0.578 W/kg in a 10-g tissue. The corresponding SARs for the MSHIS-added (JCHIS-added) antenna are 0.037 W/kg (0.038 W/kg) and 0.031 W/kg (0.036 W/kg), respectively. The reduction due to the HISs is significant, further supporting that the MSHIS and JCHIS can be used as an electromagnetic protection screen.

For further comparison, the measured SARs of a 2.45-GHz coax-fed microstrip patch antenna are also listed in Table 4. The 30-mm-long and 7.5-mm-wide radiating patch was printed on a 1.6-mm-thick grounded square FR4 substrate with a side length of 75 mm. The SARs of the patch antenna are 0.036 W/kg in a 1-g tissue and 0.030 W/kg in a 10-g tissue. It was found that a well-designed patch antenna, because of its large ground plane, can also very effectively reduce the SAR [34]. However, many practical antennas (e.g., monopole, whip, meander, and helical antennas) of modern portable devices do not have the properties of low BRP and SAR. Therefore, the EM protection screens are particularly useful for these antennas.

5. CONCLUSION

In this study, the characteristics of the MSHIS and JCHIS have been numerically analyzed and verified by measurement. It was found that the GTEM method can best predict the resonant frequency of the HISs and the microstrip line method can best provide the resonant bands of the HISs.

The effects of adding a finite high-impedance screen to a monopole antenna have been thoroughly studied for the application of 2.4 GHz WLAN band. The study results revealed the HISs can narrow and shift the operating band of the monopole antenna. Hence, with the HISs appropriately designed, the bandwidths of the HIS-added antennas can be adjusted, and the out-of-band spurious emissions from the wireless device can be reduced. Both the MSHIS and JCHIS can achieve the declared influence on the monopole antenna with the same number of HIS cells, but the influence of the MSHIS seems to be more stable as the number of cells is varied. In addition, the study results also indicated that the HISs can reduce the backward radiation power of the monopole antenna by approximately 10 dB without affecting the forward radiation power. The measured SARs have been greatly reduced from 0.976 W/kg in a 1-g tissue and 0.578 W/kg in a 10-g tissue for the monopole antenna to 0.037 W/kg (0.038 W/kg) and 0.031 W/kg (0.036 W/kg), respectively, if an MSHIS (JCHIS) is employed as the electromagnetic protection screen.

ACKNOWLEDGMENT

The authors deeply thank the reviewers for their helpful comments and valuable suggestions. The authors also thank Telecommunication Laboratories of Chunghwa Telecom Company for their support in the SAR measurement using their Aprel ALSAS 10 SAR testing system. This work was supported by the National Science Council of Taiwan, R.O.C., under Grant NSC-98-2221-E-224- 011-MY2.

REFERENCES

1. IEEE Std. C95.1-2005, *IEEE Standard for Safety Levels with Respect to Human Exposure to Radio Frequency Electromagnetic Fields, 3 kHz to 300 GHz*, IEEE, New York, 2005.
2. ICNIRP, "International commission on non-ionizing radiation protection guidelines for limiting exposure to time-varying electric, magnetic, and electromagnetic fields (up to 300 GHz)," *Health Phys.*, Vol. 74, No. 4, 494–522, Apr. 1998.

3. FCC OET Bulletin 65, Supplement C, "Evaluating compliance with FCC guidelines for human exposure to radiofrequency electromagnetic fields," Jun. 2001.
4. BS EN 62209-1: 2006, "Human exposure to radio frequency fields from hand-held and body-mounted wireless communication devices — Human models, instrumentation, and procedures — Part 1: Procedure to determine the specific absorption rate (SAR) for hand-held devices used in close proximity to the ear (frequency range of 300 MHz to 3 GHz)," Sep. 2006.
5. IEEE Std. 1528–2003, "IEEE recommended practice for determining the peak spatial-average specific absorption rate (SAR) in the human head from wireless communications devices: Measurement techniques," Dec. 2003.
6. Kivekas, O., J. Ollikainen, T. Lehtiniemi, and P. Vainikainen, "Bandwidth, SAR, and efficiency of internal mobile phone antennas," *IEEE Trans. on Electromagnetic Compatibility*, Vol. 46, No. 1, 71–86, Feb. 2004.
7. Kusuma, A. H., A.-F. Sheta, I. Elshafiey, Z. Siddiqui, M. A. S. Alkanhal, S. Aldosari, S. A. Alshebeili, and S. F. Mahmoud, "A new low SAR antenna structure for wireless handset applications," *Progress In Electromagnetics Research*, Vol. 112, 23–40, 2011.
8. Jensen, M. A. and Y. Rahmat-Samii, "EM interaction of handset antennas and a human in personal communications," *IEEE Proceedings*, Vol. 83, No. 1, 7–17, Jan. 1995.
9. Sager, M., M. Forcucci, and T. Kristensen, "A novel technique to increase the realized efficiency of a mobile phone antenna placed beside a head-phantom," *IEEE Antennas and Propagation Society International Symposium*, Vol. 2, 1013–1016, Columbus, Ohio, USA, Jun. 2003.
10. Kwak, S. I., D.-U. Sim, J. H. Kwon, and H. D. Choi, "Comparison of the SAR in the human head using the EBG structures applied to a mobile handset," *European Microwave Conference*, 937–940, Munich, European, Oct. 2007.
11. Chou, H.-H., H.-T. Hsu, H.-T. Chou, K.-H. Liu, and F.-Y. Kuo, "Reduction of peak SAR in human head for handset applications with resistive sheets (r-cards)," *Progress In Electromagnetics Research*, Vol. 94, 281–296, 2009.
12. Islam, M. T., M. R. I. Faruque, and N. Misran, "Design analysis of ferrite sheet attachment for SAR reduction in human head," *Progress In Electromagnetics Research*, Vol. 98, 191–205, 2009.
13. Sievenpiper, D. F., L. Zhang, R. F. J. Broas, N. G. Alexopolous,

and E. Yablonovitch, "High-impedance electromagnetic surfaces with a forbidden frequency band," *IEEE Trans. on Microwave Theory and Technique,* Vol. 47, No. 11, 2059–2074, Nov. 1999.

14. Sievenpiper, D. F., *High-Impedance Electromagnetic Surfaces*, Ph.D. Dissertation, University of California, Los Angeles, USA, 1999.
15. Kollatou, T. and C. Christopoulos, "Use of high-impedance surfaces in electromagnetic compatibility applications," *IEEE Trans. on Magnetics*, Vol. 45, No. 3, 1812–1815, Mar. 2009.
16. Munk, B. A., *Frequency Selective Surfaces: Theory and Design*, Wiley, Hoboken, NJ, 2000.
17. Guo, C., H.-J. Sun, and X. Lv, "A novel dualband frequency selective surface with periodic cell perturbation," *Progress In Electromagnetics Research B*, Vol. 9, 137–149, 2008.
18. Costa, F., S. Genovesi, and A. Monorchio, "On the bandwidth of high-impedance frequency selective surfaces," *IEEE Antennas Wireless and Propagation Letters*, Vol. 8, 1341–1344, 2009.
19. Lee, Y. L. R., A. Chauraya, D. S. Lockyer, and J. C. Vardaxoglou, "Dipole and tripole metallodielectric photonic bandgap (MPBG) structures for microwave filter and antenna applications," *IEE Proc. Optoelectronics*, Vol. 147, No. 6, 395–400, Dec. 2000.
20. Poilasne, G., "Antennas on high impedance ground planes: On the importance of the antenna isolation," *Progress In Electromagnetics Research*, Vol. 41, 237–255, 2003.
21. Feresidis, A. P., G. Goussetis, S. Wang, and J. C. Vardaxoglou, "Artificial magnetic conductor surfaces and their application to low-profile high-gain planar antennas," *IEEE Trans. on Antennas and Propagations*, Vol. 53, No. 1, 209–215, Jan. 2005.
22. Jing, L. and H-Y. D. Yang, "Radiation characteristics of a microstrip patch over an electromagnetic bandgap surface," *IEEE Trans. on Antennas and Propagations*, Vol. 55, No. 6, 1691–1697, Jun. 2007.
23. Zheng, Q.-R., Y.-M. Yan, X.-Y. Cao, and N.-C. Yuan, "High impedance ground plane (HIGP) incorporated with resistance for radar cross section (RCS) reduction of antenna," *Progress In Electromagnetics Research*, Vol. 84, 307–319, 2008.
24. Tomeo-Reyes, I. and E. Rajo-Iglesias, "Comparative study on different his as ground planes and its application to low profile wire antennas design," *Progress In Electromagnetics Research*, Vol. 115, 55–77, 2011.
25. Xie, H.-H., Y.-C. Jiao, L.-N. Chen, and F.-S. Zhang, "An effective

analysis method for EBG reducing patch antenna coupling," *Progress In Electromagnetics Research Letters*, Vol. 21, 187–193, 2011.

26. Chang, C.-S., M.-P. Houng, D.-B. Lin, K.-C. Hung, and I.-T. Tang, "Simultaneous switching noise mitigation capability with low parasitic effect using aperiodic high-impedance surface structure," *Progress In Electromagnetics Research Letters*, Vol. 4, 149–158, 2008.
27. Chang, C.-S., J.-Y. Li, W.-J. Lin, M.-P. Houng, L.-S. Chen, and D.-B. Lin, "Controlling the frequency of simultaneous switching noise suppression by using embedded dielectric resonators in high-impedance surface structure," *Progress In Electromagnetics Research Letters*, Vol. 11, 149–158, 2009.
28. Lin, M. S., C. H. Huang, and C-I. G. Hsu, "Techniques of evaluating high impedance surfaces used for SAR reduction," *Asia-Pacific Symposium on Electromagnetic Compatibility*, 210–213, Beijing, China, Apr. 2010.
29. Remski, R. T., "Analysis of photonic bandgap surfaces using ansoft HFSS," *Microwave Journal*, Vol. 53, 190–198, Sep. 2000.
30. Chen, Z. N., *Antennas for Portable Devices*, Wiley, New York, 2007.
31. CTIA Certification Program Management Document, "Test plan for mobile station over the air performance, method of measurement for radiated RF power and receiver performance," Revision 3.0, Dec. 2009.
32. FCC CFR 47, Part 15, "Radio frequency devices," Feb. 2006.
33. Aprel ALSAS 10 Universal system. Available at www.aprel.com.
34. Bouhorma, M., F. Elouaai, and A. Mamouni, "Computation of SAR for two antennas used in mobile communication systems: monopole and patch," *New Technologies, Mobility and Security, NTMS'08*, 1–4, Nov. 2008.